THE JOURNAL OF BIOLOGICAL CHEMISTRY VOL. 288, NO. 34, pp. 24528–24539, August 23, 2013

The STRA6 Receptor Is Essential for Retinol-binding Protein-induced Insulin Resistance but Not for Maintaining Vitamin A Homeostasis in Tissues Other Than the Eye*

Received for publication, May 8, 2013, and in revised form, July 1, 2013 Published, JBC Papers in Press, July 9, 2013, DOI 10.1074/jbc.M113.484014

Daniel C. Berry[‡§1,2], Hugues Jacobs[¶‖1,3], Gurdeep Marwarha[‡], Aurore Gely-Pernot[¶], Sheila M. O'Byrne[**], David DeSantis[§], Muriel Klopfenstein[¶], Betty Feret[¶], Christine Dennefeld[¶], William S. Blaner[**], Colleen M. Croniger[§], Manuel Mark[¶], Noa Noy[‡§4], and Norbert B. Ghyselinck[¶5]

From the Departments of [‡]Pharmacology and [§]Nutrition, Case Western Reserve University School of Medicine, Cleveland, Ohio 44106, the [¶]Institut de Génétique et de Biologie Moléculaire et Cellulaire, CNRS (UMR7104), INSERM U964, Université de Strasbourg, F-67404 Illkirch, France, the [‖]Institut Clinique de la Souris, F-67404 Illkirch, France, and the [**]Department of Medicine, College of Physicians and Surgeons, Columbia University, New York, New York 10032

Background: STRA6 transports retinol into cells and activates cell signaling.
Results: Ablation of *Stra6* does not impair vitamin A homeostasis in tissues other than the eye but protects mice against RBP-induced insulin resistance.
Conclusion: One major function of STRA6 is to control cell signaling.
Significance: The data point at a new function for vitamin A and its blood carrier RBP.

The plasma membrane protein STRA6 is thought to mediate uptake of retinol from its blood carrier retinol-binding protein (RBP) into cells and to function as a surface receptor that, upon binding of holo-RBP, activates a JAK/STAT cascade. It was suggested that STRA6 signaling underlies insulin resistance induced by elevated serum levels of RBP in obese animals. To investigate these activities *in vivo*, we generated and analyzed *Stra6*-null mice. We show that the contribution of STRA6 to retinol uptake by tissues *in vivo* is small and that, with the exception of the eye, ablation of *Stra6* has only a modest effect on retinoid homeostasis and does not impair physiological functions that critically depend on retinoic acid in the embryo or in the adult. However, ablation of *Stra6* effectively protects mice from RBP-induced suppression of insulin signaling. Thus one biological function of STRA6 in tissues other than the eye appears to be the coupling of circulating holo-RBP levels to cell signaling, in turn regulating key processes such as insulin response.

Vitamin A (retinol, ROH)[6] is indispensable for embryonic development, vision, reproduction, and post-natal life in vertebrates (1, 2). With the exception of vision, which relies on 11-*cis*-retinaldehyde, the biological actions of vitamin A are mediated by its metabolite retinoic acid (RA), which functions by activating specific nuclear receptors (3, 4). ROH is stored in various tissues, including white adipose tissue (WAT), lung, and retinal pigment epithelium (RPE) in the eye, but its major storage pool is found in the liver. It is secreted from hepatocytes bound to retinol-binding protein (RBP), a 21-kDa carrier encoded by the *Rbp4* gene (5). RBP-bound ROH (holo-RBP) accounts for the predominant fraction of retinoids in blood during fasting but, in postprandial periods, the amount of ROH that circulates as retinyl esters in chylomicrons can greatly exceed that bound to RBP (5). Hence, an important physiological role of RBP is to mobilize ROH from hepatic stores to peripheral tissues when dietary vitamin A intake is low (6, 7). Accordingly, *Rbp4*-null mice fed a vitamin A-deficient diet develop characteristic symptoms of vitamin A deficiency (VAD) (8). Interestingly, it has been reported that plasma level of RBP increases in obese mice and humans and that the elevated serum levels of the protein markedly suppress insulin responses (9). Thus, RBP may link obesity and insulin resistance.

Two models have been proposed to account for uptake of ROH from holo-RBP by target cells (reviewed in Ref. 10). According to one model, ROH spontaneously dissociates from RBP and, due to its lipophilic nature, moves into cells by diffusion across the plasma membranes at fluxes that are dictated by its extracellular to intracellular concentration gradient (11, 12). Another model proposes that uptake of ROH into cells is mediated by a cell-surface receptor for holo-RBP (13, 14). In keeping with this notion, it was recently shown that a plasma membrane protein termed STRA6 binds extracellular holo-RBP and transports ROH into cultured cells (15). STRA6 is a multitransmembrane domain-containing protein expressed in various tissues and is most highly expressed in retinal pigment epithelium (RPE) in the eye (15, 16). It has been reported that, in humans, mutations in the *Stra6* gene correlate with the occurrence of a Matthew-Wood syndrome (17, 19), a severe polymalformative

* This work was supported, in whole or in part, by National Institutes of Health Grant R01 DK088669 (to N. N.). This work was also supported by CNRS, Inserm, and Hôpital Universitaire de Strasbourg grants (to M. M. and N. B. G.).
[1] Both authors equally contributed to this work.
[2] Supported in part by National Institutes of Health Grant T3 DK073195.
[3] Supported by grants from the French Ministry of Research and Technology and Fondation pour la Recherche Médicale Grant FDT20080914176.
[4] To whom correspondence may be addressed. Fax: 216-368-1300; E-mail: noa.noy@case.edu.
[5] To whom correspondence may be addressed. Fax: 33-388-653-201; E-mail: norbert@igbmc.fr.
[6] The abbreviations used are: ROH, retinol; GIR, glucose infusion rate; HFHSD, high fat/high sucrose diet; IR, insulin receptor; RA, retinoic acid; RBP, retinol-binding protein; RPE, retinal pigment epithelium; VAD, vitamin A deficiency; VADD, vitamin A deficient diet; WAT, white adipose tissue.

congenital disease that includes as main characteristics microphthalmia, pulmonary hypoplasia, heart defects, and diaphragmatic hernia. In contrast to *Stra6*, mutations in the *Rbp4* gene in humans lead to only mild clinical symptoms traceable to VAD, including night blindness and a modest retinal dystrophy (20). The observations that RBP mutations give rise to much less severe defects than those yielded by STRA6 mutations suggest either that STRA6 exerts biological functions independently of its role as an RBP receptor or that Matthew-Wood syndrome originates from chromosomal aberrations other than STRA6 mutations.

Our recent studies using cultured cell models revealed that, in addition to mediating ROH uptake, STRA6 functions as a cytokine receptor that triggers a signaling cascade in response to holo-RBP. Specifically, we found that binding of holo-RBP to STRA6 results in recruitment of JAK2 that, in turn, catalyzes phosphorylation of a tyrosine residue in the cytosolic domain of STRA6, leading to recruitment and activation of the transcription factor STAT5 (21–24). As STAT target genes in WAT and muscle include *Suppressor of cytokine signaling 3* (*Socs3*), a potent inhibitor of the insulin receptor (IR) (25), these findings provided a rationale for understanding how elevated serum levels of RBP in obese animals induce insulin resistance (9).

To investigate whether STRA6 mediates ROH uptake and/or holo-RBP-induced signaling *in vivo*, we generated and analyzed the phenotype of a mouse line harboring a *Stra6*-null mutation. We show that, with the exception of RPE cells in the eye (26), ablation of *Stra6* does not greatly impact the retinoid content of tissues and does not disrupt physiological functions that are critically dependent on RA in the embryo or in the adult, even under conditions of VAD. Hence, although contributing in part to ROH uptake by cells, STRA6 does not appear to be mandatory for normal development in the mouse and for ROH availability *in vivo* in tissues other than the eye. In contrast, ablation of *Stra6* abolished the ability of holo-RBP to activate a JAK/STAT cascade and to induce insulin resistance.

EXPERIMENTAL PROCEDURES

Mouse Studies—Mice were housed according to Animal Research Committee (ARC) protocol (United States) or in a facility licensed by the French Ministry of Agriculture (agreement number B67-218-5). Animal experiments were supervised by M. M. and N. B. G. (agreements numbers 67-62 and 67-205), in compliance with the European legislation on care and use of laboratory animals. Mice with a mixed C57BL/6-129/Sv (50–50%) genetic background were maintained on a 12-h light and dark cycle on a normal chow diet. Noon of the day of a vaginal plug was taken as embryonic day 0.5 (E0.5). Embryos and fetuses were collected by caesarean section, and the yolk sacs were taken for DNA extraction. The breeding diets (D03 from Usine d'Alimentation Rationnelle (UAR) in France, or Diet 5P76 from LabDiet in the United States) contained 25,000–29,000 IU of vitamin A per kg. The mice had access to water and diet *ad libitum*. The high fat/high sucrose diet contained 35% (w/w) fat (D12331 from Research Diets). For vitamin A depletion studies performed in the United States and destined for HPLC analysis of retinoid contents, 12-week-old control (wild type, WT) and *Stra6*-null mutant mice were fed a diet devoid of vitamin A (Research Diet AIN93G-D13110GC) for 4 weeks. For vitamin A depletion studies performed in France and destined for morphological analyses, 6-week-old $Rbp4^{+/+}$ and $Rbp4^{-/-}$ mice as well as $Stra6^{+/+}$ and $Stra6^{L-/L-}$ mice were fed the same vitamin A-deficient diet (Harlan TD86143) for 7 weeks.

Generation of Stra6-null Mice and Genotyping—The targeting vector was constructed as follows (see Fig. 1*A*): an ~1-kb-long DNA fragment encompassing the XbaI-AjiI region of *Stra6* locus and containing exons E5 to E7 was amplified by PCR from 129/SvPas mouse genomic DNA. It was inserted between two *lox*P sites into a Mouse Clinic Institute (Illkirch, France) proprietary vector, resulting in step 1 plasmid. This vector additionally displays an *FRT*-flanked neomycin resistance cassette (*neo*) located downstream of the second *lox*P site. Then, two ~3-kb-long genomic DNA fragments containing exon E3-E4 and exon E8 were amplified by PCR and sequentially inserted into step 1 plasmid upstream of the first *lox*P site and downstream of *neo*, respectively. The resulting targeting vector was electroporated into 129S2/SvPas mouse embryonic stem (ES) cells. After selection, targeted clones were screened by PCR using external primers. One clone targeted as expected (K126) was identified and further confirmed by Southern blot with 5′ and 3′ external probes (L3 allele; see Fig. 1*A*, $Stra6^{+/L3}$). Clone K126 ($Stra6^{+/L3}$) was injected into C57BL/6 blastocysts, and one chimera transmitted the conditional allele to the germ line. Removal of the neo cassette from the *Stra6* locus was achieved by crossing $Stra6^{+/L3}$ mice with *Actb-FLPe* transgenics (*Tg*(*ACTFLPe*)*9205Dym*) that express FLPe recombinase in the germ line (27), thereby generating mice bearing the conditional, *lox*P-flanked, L2 allele (see Fig. 1*A*, $Stra6^{+/L2}$). Deletion of *neo* was assessed using primers 5′-GGTTCTCCGGCCGCTTGGGT-3′ and 5′-GAAGGCGATGCGCTGCGAAT-3′ that amplify a 740-bp-long fragment from *neo*. Segregation of *Actb-FLPe* transgene was assessed using primers 5′-GGAGAAAGCATCTGGGAGATCACTG-3′ and 5′-CACAACATTGGTCAGCTCTGTCAGGCC-3′, which amplify a 530-bp-long fragment from *FLPe*. Heterozygous ($Stra6^{+/L2}$) inter-crosses yielded a Mendelian ratio of WT and homozygous ($Stra6^{L2/L2}$) mice that grew normally and were healthy, fertile, and externally undistinguishable from WT littermates, indicating that the presence of *lox*P sites at the *Stra6* locus had no effects. The $Stra6^{+/L2}$ mice were then crossed with *CMV-Cre* transgenic mice (*Tg*(*CMV-cre*)*1Ipc*), which express Cre recombinase in the one-cell stage embryo (28), to generate mice bearing the excised, null, L− allele (see Fig. 1*A*, $Stra6^{+/L-}$). They were genotyped by PCR analysis of tail DNA (Fig. 1*B*) using primers 1 (5′-ACTGACAGATCTATTCAGGAGGAGG-3′) and 2 (5′-AGGGGAGGATCCTTTCACCACC-3′; see Fig. 1*A*) to amplify the wild-type (172 bp long) and the *lox*P-flanked L2 (222 bp long) alleles, or primers 1 and 3 (5′-GCATCCTCTTCCTCCACTCTGC-3′) to amplify the L− allele (350 bp long). Conditions were two cycles with denaturation for 1 min at 94 °C, annealing for 1 min at 61 °C, and elongation for 1 min at 72 °C, followed by 30 cycles with denaturation for 30 s at 92 °C, annealing for 30 s at 61 °C, and elongation for 30 s at 72 °C. Segregation of *CMV-Cre* transgene was assessed using primers 5′-ATTTGCCTGCATTACCGGTC-3′ and 5′-ATCAACGT-

TTTCTTTTCGGA-3′, which amplify a 350-bp-long fragment from *Cre*.

Proteins and Immunoblotting—Recombinant RBP was expressed in *Escherichia coli* and purified as described previously (21). Endotoxin levels were measured using *Limulus amebocyte* lysate (LAL) assay for endotoxin content (Pierce LAL chromogenic endotoxin quantitation kit, catalog number 88282). COS-7 cells were grown at 37 °C with 5% (v/v) CO_2 in DMEM supplemented with 5% (v/v) fetal calf serum and 40 μg/ml gentamicin. They were transfected with expression plasmids containing full-length coding sequences for *E. coli lacZ* (in pCH110, Amersham Biosciences), mouse *Stra6* (in pReceiver-M01, GeneCopoeia), or mouse *Rbpr2* (1300002K09Rik-001 in pSG5, Stratagene) using JetPEI transfection reagent (Polyplus-Transfection SA). To extract proteins, embryo tissues and transfected cells were lysed and incubated for 30 min on ice in RIPA buffer (50 mM Tris-HCl, pH 7.5, 150 mM NaCl, 0.5% (w/v) sodium deoxycholate, 1% (v/v) Nonidet P-40, 0.2% (w/v) SDS) supplemented with an anti-protease mixture (Roche Diagnostics). Protein extracts were resolved by 12% (w/v) SDS-PAGE and blotted onto nitrocellulose membranes (Schleicher & Schuell) according to standard procedures. STRA6 protein was detected using a rabbit polyclonal antibody (RP-S6, diluted 1:1000) generated at Institut de Génétique et de Biologie Moléculaire et Cellulaire and directed against the C-terminal part of mouse STRA6 (amino acids 586–615; CALLLHAP-SPQPRPPLAPQDSLRPAEEEEG). Immunoreactions were visualized using protein A coupled to horseradish peroxidase (HRP; diluted 1:5000), followed by chemiluminescence using Immobilon Western Chemiluminescent HRP Substrate (Millipore) according to the manufacturer's protocol. Antibodies against AKT, pAKT, IR, pIR, JAK2, and pJAK2 were from Cell Signaling and used as described (21). Anti-actin and anti-tubulin antibodies were from Santa Cruz Biotechnology. Antibodies against RBP and β-galactosidase (β-gal) were from Dako and Capel, respectively.

Histology, in Situ Hybridization, Immunohistochemistry, and β-Galactosidase Activity Analysis—Tissue collection and systematic histopathology were as described previously (29). Briefly, samples were fixed in 10% (v/v) formalin for 16 h, except for testis, which was fixed in Bouin's fluid for 16 h. All samples were embedded in paraffin, and 5-μm-thick sections were stained with either hematoxylin and eosin or periodic acid-Schiff. *In situ* hybridizations were performed as described (30). For immunodetection of STRA6, 10-μm-thick sections of unfixed frozen tissues were incubated in cold acetone (−20 °C, 5 min), air-dried, hydrated in phosphate-buffered saline (PBS), and fixed for 10 min in ice-cold 4% (w/v) paraformaldehyde in PBS. Sections were incubated for 1 h with the anti-STRA6 antibody diluted 1:1000 in PBS. Detection of bound primary antibodies was achieved by incubating the section for 45 min at room temperature with a Cy3-conjugated goat anti-rabbit IgG (Biomol ImmunoResearch Laboratories, Exeter, UK) diluted 1:1000 in PBS. The sections were counterstained with 0.001% (w/v) 4,6-diamidino-2-phenylindole dihydrochloride (DAPI). For detection of β-gal activity, embryos and fetuses were fixed in 0.2% (w/v) glutaraldehyde, 2% (w/v) paraformaldehyde, 0.01% (v/v) sodium deoxycholate, 0.02% Nonidet P-40, 5 mM EGTA, and 2 mM $MgCl_2$ in PBS at 4 °C for 1 h, rinsed in PBS for 15 min, and then stained as described previously (31) for 1.5 h at 30 °C. They were post-fixed either in 4% (w/v) paraformaldehyde in PBS or in Bouin's fluid for 16 h and embedded in paraffin, and 5-μm-thick sections were counter-stained with neutral red.

High Performance Liquid Chromatography (HPLC) Analysis of Retinoids—Reverse phase HPLC analysis of ROH and retinyl esters in tissues was performed as described previously (32, 33). Retinoids (ROH, retinyl palmitate, oleate, linoleate, and stearate) were identified using a Waters 2996 photodiode array detector to compare retention times and spectral data of experimental compounds with those of authentic standards. Concentrations of ROH and retinyl esters were quantitated by comparing integrated peak areas of the unknowns against those of known amounts of purified standards.

Uptake of ROH from Holo-RBP into Target Tissues in Vivo—Following the procedure described in Ref. 34, 8-week-old mice were intraperitoneally injected with 0.2 mg of holo-RBP containing 0.02 mCi of [^{3}H]ROH-RBP (total volume 60 μl), and 2 h post-injection a blood sample was collected, and hearts were perfused with 0.9% saline to remove blood containing [^{3}H]ROH. Tissues were isolated, weighed, and homogenized in phosphate-buffered saline, and radioactivity was measured by scintillation counting. Counts were normalized per g of tissue.

Insulin Measurement—Blood was collected by heart puncture, and plasma was isolated using Microtainer plasma separator tubes (BD Biosciences). Insulin was measured using an ultrasensitive mouse insulin enzyme-linked immunosorbent assay (Mercodia, Lincoln Park, MO).

Glucose and Insulin Tolerance Tests—Mice were fasted for 12 h and injected intraperitoneally with glucose (2 g kg^{-1} body weight) or insulin (0.9 units kg^{-1} body weight; Sigma). Blood was sampled from the tail vein, and glucose was measured using an UltraTouch or Accu-Chek Performa glucometers.

Lipolysis—3T3-L1 preadipocytes were induced to differentiate as described previously, and differentiation was confirmed by Oil Red-O staining and by an increase in expression of the mature adipocyte marker FABP4 (21). Note that STRA6 is only expressed in 3T3-L1 cells differentiated into adipocytes (21). Primary adipocytes were isolated as described previously (35). For lipolysis analysis, adipocytes were treated with 3-isobutyl-1-methylxanthine (0.5 mM) for 8 h. Concentration of glycerol in the media was measured using Zen-bio lipolysis kit LIP-1-NC.

Glucose Uptake—Primary adipocytes were pretreated with 1 μM holo-RBP for 12 h. Cells were then treated with insulin (5 mM, 15 min), and 25 mM 2-[1,2-^{3}H]deoxy-D-glucose was added. 15 min later, cells were solubilized in 0.5 mM NaOH and neutralized with glacial acetic acid. Radioactivity in lysates was measured by scintillation counting (Beckman Coulter).

Hyperinsulinemic-Euglycemic Clamp—For each mouse a femoral vein catheter was placed under pentobarbital (12% w/v) anesthesia 3 days prior to the experiment. The clamp test was conducted after a 5-h fasted vigil and not on restrained male mice ($n = 9$ or 10/group). Insulin was administered at 18 mUI/kg·min (Sigma) to raise plasmatic insulin concentration, and glucose was infused through the catheter to maintain euglycemia, which was determined every 5 min on blood drops obtained by tail tip puncture and analyzed with a glucometer

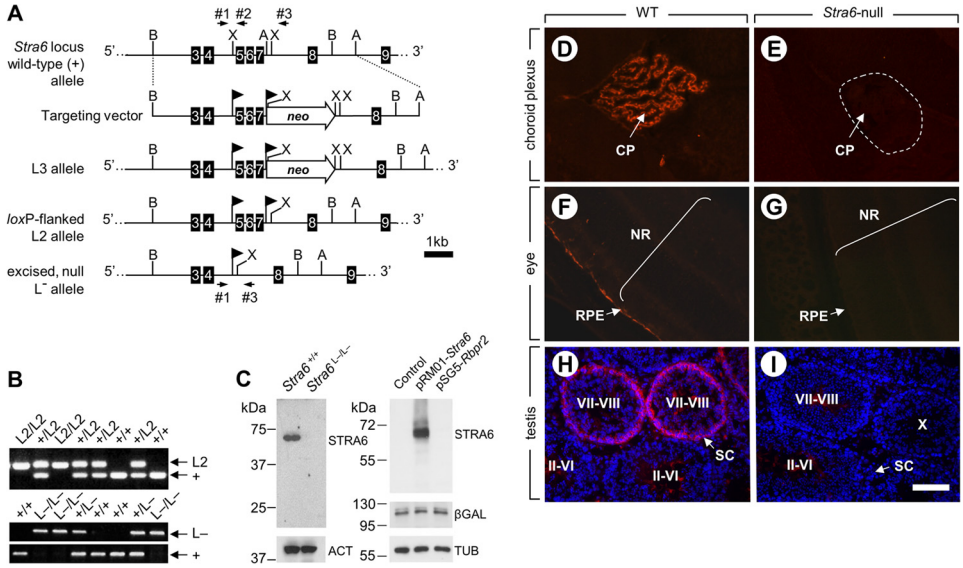

FIGURE 1. **Targeted disruption of the *Stra6* gene.** *A,* structure of the targeting vector and partial restriction maps of the WT *Stra6* locus before ((+) allele) and after (L3 allele) homologous recombination, as well as after FLPe- and Cre-mediated excision (L2 and L− alleles, respectively). *Numbered black boxes* indicate exons. The locations of restriction sites (*A,* AijI; *B,* BclI; *X,* XbaI) are indicated. *Arrowhead flags* represent *loxP* sites; *neo*, *FRT*-flanked neomycin resistance cassette. *Arrows* indicate the location and orientation of PCR primers 1–3. *B,* PCR analysis of tail genomic DNA from mice with the indicated genotype using primers 1 and 2 (*upper panel*) and 1–3 (*lower panel*). The identities of the different alleles are indicated on the *right*. *C, left panel,* immunoblots of STRA6 in protein extracts from E9.5 embryos with the indicated *Stra6* genotype, attesting for the lack of STRA6 in the mutant sample. Control for protein loading was assessed using anti-actin antibodies (*ACT*). *Right panel,* immunoblot of STRA6 in lysates from COS-7 cells transfected with plasmids driving expression of either STRA6 or RBPR2, as indicated, attesting for the specificity of the anti-STRA6 antibody. Controls for protein loading and transfection efficiency were assessed using anti-tubulin (*TUB*) and anti-β-gal antibodies, respectively. *D–I,* immunodetection of STRA6 (*red signal*) on histological sections from WT (*D, F,* and *H*) and *Stra6*-null (*E, G,* and *I*) choroid plexuses (*D* and *E*), eyes (*F* and *G*), and testes (*H* and *I*). Cell nuclei were counterstained with DAPI (*H* and *I*). Note that the faint signals detected in the center of the seminiferous tubules at stages II–VI and VII–VIII in control (*H*) and in mutant (*I*) testes correspond to an unspecific staining of elongated spermatids. *CP,* choroid plexus; *RPE,* retinal pigment epithelium; *SC,* Sertoli cell; *NR*, neural retina. The *dotted line* (*E*) encircles a choroid plexus. *Brackets* (*F* and *G*) encompass the neural retinal layers. *Roman numerals* (*H* and *I*) indicate stages of the seminiferous epithelium cycle. *Scale bar* is shown in *I* and is 150 μm for *D* and *E*, 110 μm for *F* and *G*, and 100 μm for *H* and *I*.

(Accu-check, Roche Diagnostics) (36). The average glucose infusion rate (GIR) was calculated when both glycemia and hyperinsulinemia were set at constant levels over a period of 60 min.

Analysis of mRNA and of Gene Expression—Cellular mRNA was extracted using TRIzol reagent (Invitrogen). Tissue mRNA was extracted using RNeasy lipid tissue minikit (Qiagen) or RNeasy fibrous tissue minikit (Qiagen), and cDNA was generated by using GeneAmp RNA PCR (Applied Biosystems) or QuantiTect reverse transcription kit (Qiagen) according to the manufacturer's instructions. To assess for gene expression in WAT, skeletal muscle, and liver, quantitative real time PCR was carried out on cDNA by using TaqMan chemistry and Assays-on-Demand probes (Applied Biosystems) for *Socs3* (Mm01249143), *Pparg* (Mm00440945_m1), and 18 S rRNA. To assess for *Stra6* and *Rbpr2* (1300002K09Rik) expression, quantitative real time PCR was carried out on cDNA by using SYBR Green (Roche Diagnostics) with primers 5′-GTCATCGCGGACTTGGAC-3′ and 5′-TTGATGCTGCAGTGAGGTTC-3′ for *Stra6*, and 3′-TCCTGGGGAACCACTTTGGA-3′ and 5′-CCATGCCTCCGATGAAAAGC-3′ for *Rbpr2*. Data were normalized to the level of *Arbp0* mRNA, whose expression was not altered by *Stra6* ablation. Statistical analyses were carried out using two-tail Student's *t* test unless specified otherwise.

RESULTS

STRA6 Is Not Essential for Maintaining Vitamin A Homeostasis, Except in the Eye—To generate mice in which the *Stra6* gene can be selectively ablated in a given tissue, exons E5 to E7 of the *Stra6* gene were flanked by *lox*P sites through homologous recombination in embryonic stem cells (Fig. 1*A*). If an aberrant splicing occurs between exons E4 and E8 of the mutant L− allele, it generates a transcript containing a frameshift mutation in the *Stra6* coding sequence that yields a stop codon 60 bp downstream of the splice acceptor site. The resulting truncated STRA6 peptide is, if synthesized, composed of the first 88 amino acid residues and is therefore not functional as it lacks 10 of the 11 transmembrane domains, the holo-RBP-binding loop, and the cytosolic domain containing the tyrosine residue phosphorylated by JAK2 (37). The $Stra6^{+/L2}$ mice were inter-crossed, and their progeny were identified by PCR analysis of tail DNA (Fig. 1*B*, *upper panel*). They were then crossed with Cre recombinase-expressing deleter mice (28) to generate heterozygotes bearing the excised, null, L− allele (Fig. 1*A*). These $Stra6^{+/L-}$ mice were inter-crossed, and their progeny were identified by PCR analysis of tail DNA (Fig. 1*B*, *lower panel*). Homozygous mutants ($Stra6^{L-/L-}$) were obtained at Mendelian frequency and appeared healthy. Immunoblot analysis using an antibody directed against a C-terminal epitope of STRA6 and not reactive against the paralog of STRA6 called RBPR2 (38) showed a single band in protein extracts from E9.5 control embryos but not in extracts from *Stra6*-null littermates (Fig. 1*C*). This ruled out the possibility that a STRA6-related, N-terminal truncated protein is generated from the mutant allele. In addition, immunohistochemistry analyses detected STRA6 in epithelial cells of the choroid plexuses, the RPE, and

TABLE 1

Retinoid content in selected tissues of 12-week-old WT and *Stra6*-null male mice fed regular chow

Data are means ± S.E. (n = 7–8 for all groups, except brain where n = 3). ND = not detected. Retinoid content in the eye was already published (26).

Tissues	ROH			Retinyl ester			Retinol Eqv.		
	Wild-type	*Stra6*-null	p value	Wild-type	*Stra6*-null	p value	Wild-type	*Stra6*-null	p value
	μg/g tissue			*μg/g tissue*					
Plasma (μg/dl)	29.1 ± 12.4	26.4 ± 8.8	*0.63*	ND	ND		29.1 ± 12.4	26.4 ± 8.8	*0.63*
Adipose	0.58 ± 0.32	0.49 ± 0.22	*0.53*	1.03 ± 0.82	1.49 ± 0.9	*0.30*	0.69 ± 0.42	1.29 ± 0.63	0.65
Brain	0.29 ± 0.07	0.35 ± 0.14	*0.49*	0.14 ± 0.24	ND		0.34 ± 0.59	0.36 ± 0.14	0.96
Heart	1.51 ± 1.36	1.72 ± 1.79	*0.80*	1.43 ± 1.27	1.00 ± 0.85	*0.61*	1.98 ± 2.14	1.83 ± 1.8	0.89
Kidney	0.35 ± 0.08	0.36 ± 0.07	*0.78*	0.30 ± 0.24	0.13 ± 0.05	*0.09*	0.25 ± 0.19	0.21 ± 0.19	0.69
Liver	6.43 ± 2.87	7.55 ± 4.47	*0.60*	176.17 ± 50.89	173.39 ± 49.70	*0.92*	99.80 ± 29.42	99.44 ± 26.73	0.98
Lungs	1.98 ± 0.48	2.83 ± 1.91	*0.25*	120.24 ± 36.13	145.40 ± 58.47	*0.35*	65.71 ± 19.43	79.88 ± 32.54	0.34
Muscle	0.21 ± 0.04	0.25 ± 0.19	*0.60*	0.80 ± 0.73	0.56 ± 0.23	*0.50*	0.31 ± 0.28	0.50 ± 0.48	0.35
Pancreas	0.41 ± 0.12	0.58 ± 0.32	*0.18*	ND	ND		0.41 ± 0.12	0.58 ± 0.32	*0.18*
Spleen	0.39 ± 0.32	0.53 ± 0.45	*0.50*	0.65 ± 0.09	0.52 ± 0.24	*0.43*	0.43 ± 0.34	0.53 ± 0.44	0.63
Testis	0.11 ± 0.07	0.13 ± 0.13	*0.75*	0.49 ± 0.34	0.48 ± 0.18	*0.96*	0.49 ± 0.45	0.28 ± 0.24	*0.28*

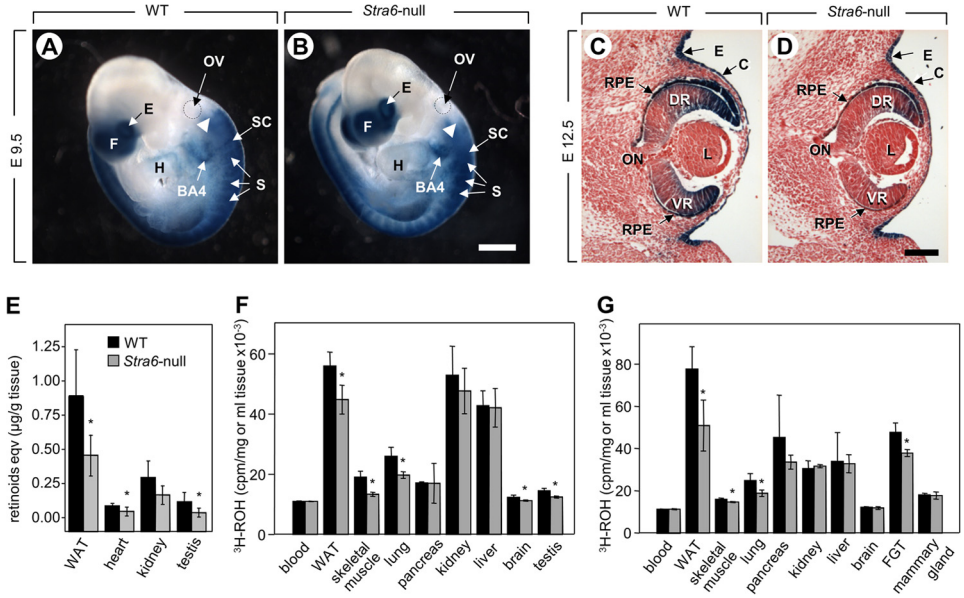

FIGURE 2. **STRA6 contributes to ROH uptake but is not critical for maintaining sufficient steady state levels of tissue ROH even under VAD.** *A* and *B*, whole mount X-Gal staining (in *blue*) of E9.5 WT and *Stra6*-null embryos harboring the *Tg(RARE-Hspa1b/lacZ)12Jrt/J* reporter transgene. *BA4*, fourth branchial arch; *E*, eye; *f*, forebrain; *H*, heart; *OV*, otic vesicle; *S*, somite; *SC*, spinal cord. The *dotted lines encircle* the otic vesicle. *Arrowheads* point to the anterior limit of the first somite. *Scale bar* in *B*, 375 μm. *C* and *D*, sagittal sections from E12.5 WT and *Stra6*-null fetuses harboring the *Tg(RARE-Hspa1b/lacZ)12Jrt/J* transgene after X-Gal staining. *C*, corneal ectoderm; *DR*, dorsal retina; *E*, ectoderm, *L*, lens; *ON*, optic nerve; *RPE*, retinal pigment epithelium; *VR*, ventral retina. *Scale bar* in *D*, 150 μm. *E*, retinoid equivalents (ROH + retinyl esters) in tissues of 16-week-old WT and *Stra6*-null males fed a VADD for 4 weeks prior to measurements (n = 7–8). *F* and *G*, [^{3}H]ROH taken up by tissues 2 h post-injection of [^{3}H]ROH-labeled holo-RBP into 8-week-old WT and *Stra6*-null male (*F*) and female (*G*) mice. *FGT*, female genital tract. Data are mean ± S.E. (n = 4/group), *, $p < 0.05$, WT *versus* *Stra6*-null mice.

Sertoli cells at stages VII–VIII of the seminiferous epithelium cycle of WT but not of *Stra6*-null mice (Fig; 1, *D–H*). Hence, the *Stra6* L− allele is indeed a null allele and *Stra6*$^{L-/L-}$ mice are hereafter designated *Stra6*-null mice.

A systematic analysis of organs (39) from adult 8-week-old *Stra6*-null males and females (n = 3 each) did not reveal any histological abnormality except in the eye, which showed a persistent and hyperplasic primary vitreous body (26). In addition, retinoid levels (ROH + retinyl ester) in most tissues were similar in WT and *Stra6*-null mice fed regular chow (Table 1), except in the RPE where a severe depletion of retinoid was observed upon ablation of STRA6 (26). To examine whether *Stra6* ablation alters local RA synthesis, the effects of the mutation were assessed in embryos harboring the *Tg(RARE-Hspa1b/lacZ)12Jrt/J* transgene (40), a reporter commonly used to monitor RA-dependent signaling (reviewed in Refs. 41, 42). At E9.5, a developmental stage at which *Stra6* is expressed in many tissues (19), WT and *Stra6*-null embryos (n = 5 each) displayed identical patterns of reporter activity (Fig. 2, *A* and *B*). At E12.5, the reporter activity in *Stra6*-null fetuses (n = 5) was normal in all RA-dependent tissues except the RPE and the ventral retina, where it was dramatically reduced (Fig. 2, *C* and *D*). Thus, with the notable exception of RPE, *Stra6* ablation does not significantly compromise ROH availability for RA signaling during *in utero* development, providing an explanation for the lack of fetal malformations other than the persistent and hyperplastic primary vitreous body (26).

If STRA6 is essential for enabling uptake of ROH from circulating holo-RBP, it may be expected that its ablation would mimic ablation of *Rbp4*, the gene coding for RBP. Feeding a vitamin A-deficient diet (VADD) to pregnant *Rbp4*-null females yields offspring suffering a fetal VAD syndrome (8). In contrast, no E14.5 *Stra6*-null fetuses (n = 6) recovered from *Stra6*$^{L-/L-}$ dams fed a VADD for 5 weeks prior to mating with

TABLE 2
Malformations in embryos exposed to excess retinol

Stra6 invalidation does not enhance fetal toxicity of ROL. A total of 135 E14.5 fetuses were obtained from 17 $Stra6^{+/L-}/Lrat^{+/L-}$ intercrosses. Female mice were dosed by oral gavage with all-*trans*-ROL diluted in sunflower oil at E9 (200 mg/kg). Exophthalmia was used as a hallmark of treatment efficiency.

	n pups	*n* litters	Exophthalmia	Craniofacial defects	Tail truncation
$Stra6^{+/+}$ $Lrat^{+/+}$	8	6	100%	0	0
$Stra6^{-/-}$ *Lrat* +/+	7	7	100%	0	0
$Stra6^{+/+}$ $Lrat^{-/-}$	8	5	100%	62.5% ($n = 5$)	62.5% ($n = 5$)
$Stra6^{-/-}$ $Lrat^{-/-}$	7	6	100%	71.4% ($n = 5$)	71.4% ($n = 5$)

$Stra6^{+/L-}$ males and throughout gestation exhibited any hallmarks of fetal VAD syndrome. Hence, *Stra6* ablation does not mimic the effects of *Rbp4* ablation in mice fed a VADD.

A previous study that used a zebrafish model led to the suggestion that STRA6 promotes ROH efflux from cells thereby protecting them from excess accumulation of the vitamin and its transcriptionally active metabolite RA (43). Therefore, *Stra6*-null fetuses should be more sensitive than WT fetuses to the teratogenic effect of excess ROH. To test for this hypothesis, $Stra6^{+/L-}$ females were mated with $Stra6^{+/L-}$ males, and then given a single oral dose of ROH (200 mg/kg) at E9.0, an embryonic stage highly sensitive to excess ROH (44) and at which *Stra6* is widely expressed (16). Examination of embryos at E14.5 revealed that WT and *Stra6*-null fetuses displayed identical malformations hallmarking ROH-induced teratogenesis (Table 2). To rule out the possibility that excess ROH was not teratogenic because of esterification by lecithin-retinol acyltransferase (45), the effects of excess ROH was also examined in *Stra6*-null embryos additionally lacking *Lrat* (46). As expected, excess ROH was highly teratogenic in the absence of lecithin-retinol acyltransferase. However, further ablating *Stra6* did not increase the potency of ROH in inducing malformations (Table 2). Finally, if STRA6 enhances efflux of ROH from cells to the circulation, it could be expected that plasma levels of ROH would be higher in STRA6-null mice. However, no differences in plasma levels of ROH were observed between WT and STRA6-null mice fed vitamin A-sufficient or -deficient diets. Taken together, the data argue against the possibility that STRA6 protects cells from ROH toxicity.

STRA6 Is Involved in ROH Uptake by Extra-hepatic Tissues in Vivo—Tissues can obtain vitamin A from holo-RBP or, during post-prandial periods, from circulating chylomicra carrying dietary retinyl esters. To examine whether the effects of STRA6 ablation may become apparent under conditions where holo-RBP is the sole source for ROH, mice were fed a VADD for 4 weeks, sufficient to abrogate supply of retinyl esters from chylomicra. Under these conditions, total retinoid levels (ROH + retinyl esters) were somewhat lower in WAT, kidney, heart, and testis of Stra6-null mice as compared with WT littermates (Fig. 2*E*). These observations suggest that, although not essential, STRA6 is nevertheless involved in uptake of ROH from holo-RBP by some tissues *in vivo*. To directly examine the effects of STRA6 on tissue uptake of ROH, RBP complexed with ^{3}H-labeled ROH was injected into WT and *Stra6*-null mice, and ROH uptake into tissues was measured 2 h post-injection. Tissues known to express STRA6, including skeletal muscle, lung, WAT, brain, testis, and female genital tract, took up less [^{3}H]ROH in *Stra6*-null than in WT mice. In contrast, *Stra6* ablation had no effect on uptake of [^{3}H]ROH by tissues that do not express the receptor, *e.g.* liver and mammary gland (Fig. 2, *F* and *G*). These observations indicate that STRA6 is involved *in vivo* in mediating some uptake of ROH from holo-RBP. The data show, however, that the contribution of STRA6-mediated transport to total ROH uptake by tissues other than the eye is rather modest and that a large fraction of ROH moves from RBP into cells independently of STRA6.

STRA6-deficient Mice Are Protected from Holo-RBP-induced Insulin Resistance—Fasting insulin levels were similar in *Stra6*-null and WT mice (Fig. 3*A*), and glucose and insulin tolerance tests did not reveal differences between their insulin sensitivity (Fig. 3, *B* and *C*). However, in accordance with the suggestion that STRA6 mediates suppression of insulin responses (21), the phosphorylation levels of IR and its downstream effector AKT were higher in WAT and muscles of *Stra6*-null mice as compared with WT counterparts (Fig. 3, *D* and *E*).

The effect of STRA6 ablation on the ability of RBP to inhibit a critical hallmark of insulin activity, *i.e.* induction of glucose uptake by adipocytes, was then examined. To this end, human RBP lacking its N-terminal secretion signal, which corresponds to circulating RBP (47), was expressed in *E. coli* and purified in the presence of ROH to obtain holo-RBP (48). The protocol typically yields holo-RBP at an ROH/RBP ratio of 0.8–1 (Fig. 3*F*). The endotoxin content of protein preparations was found to be ~0.001 units/μl, lower than that of the sterile 18 megohms of MilliQ water. As reported previously (21), recombinant holo-RBP induced phosphorylation of JAK2 in HepG2 cells, whereas apo-RBP derived from the same preparations had no effect on the phosphorylation level of the kinase (Fig. 3*G*) (21). These observations verify that the ability of holo-RBP to trigger JAK/STAT signaling did not originate from bacterial contaminations in the preparations or from residual apo-RBP but were actually from specific activity of the ROH-bound protein.

Primary adipocytes were isolated from WT and *Stra6*-null mice (35) and incubated with vehicle or 1 μM holo-RBP for 12 h. Cells were then treated with insulin (5 mM, 15 min) and subsequently with [^{3}H]glucose (25 mM, 15 min), and internalized [^{3}H]glucose was measured. The rates of insulin-induced glucose uptake by WT and *Stra6*-null adipocytes were similar (Fig. 3*H*, *black bars*), in keeping with the similar tolerance of *Stra6*-null and WT mice to glucose (Fig. 3*B*). However, adipocytes differed considerably in their responses to holo-RBP, although pretreatment with holo-RBP completely abolished the ability of insulin to enhance glucose uptake by WT adipocytes, it had no effect on insulin-stimulated glucose uptake in *Stra6*-null adipocytes (Fig. 3*H*, *gray bars*). The involvement of STRA6 in modulation of insulin responses by holo-RBP was further examined using the well established model of cultured adi-

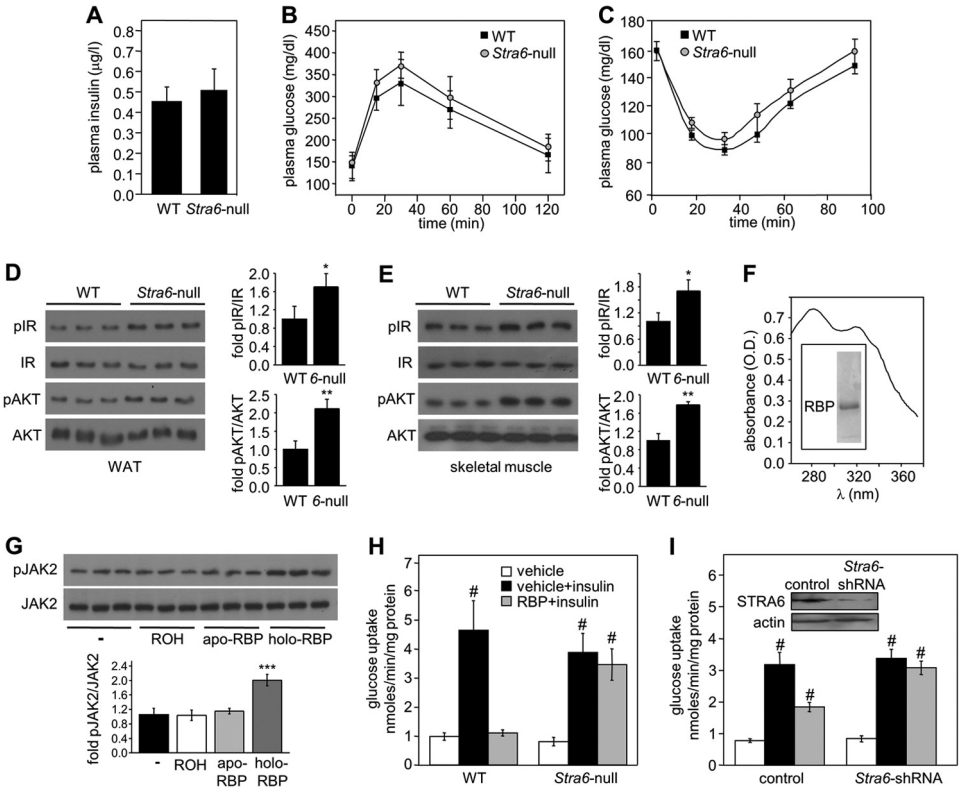

FIGURE 3. **STRA6-null adipocytes are protected from suppression of insulin signaling by holo-RBP.** *A,* plasma levels of insulin in 8-week-old WT and *Stra6*-null mice fasted for 16 h. *B,* glucose tolerance tests in 15-week-old WT and *Stra6*-null males ($n = 8$/group). *C,* insulin tolerance tests in 15-week-old WT ($n = 13$) and *Stra6*-null ($n = 15$) males. *D* and *E, left,* immunoblots of phosphorylated IR (*pIR*), total IR, phosphorylated AKT (*pAKT*), and total AKT in WAT (*D*) and skeletal muscle (*E*) of three individual 8-week-old WT and *Stra6*-null mice (*6*-null). *Right,* quantitation of immunoblots. Means ± S.D., *, $p < 0.05$; **, $p < 0.01$ *versus* WT. *F,* absorption spectrum of recombinant holo-RBP. *Inset,* purified recombinant RBP, resolved by SDS-PAGE and visualized by Commassie Blue staining. *G, top,* immunoblots of pJAK2 and JAK2 in lysates of HepG2 cells treated with buffer, 1 μM ROH, apo-RBP, or holo-RBP for 15 min. *Bottom,* quantitation of immunoblots in *A*. Data are means ± S.D. ***, $p < 0.001$ *versus* buffer-treated control (−). *H* and *I,* effect of insulin on [^{3}H]glucose uptake by adipocytes isolated from WT and *Stra6*-null males (*H*) and by 3T3-L1 adipocytes infected with empty (control) or *Stra6*-shRNA-expressing lentiviruses (*I*). *Inset* in *I,* immunoblot demonstrating reduced STRA6 expression in adipocytes infected with *Stra6*-shRNA. Assays were conducted in nontreated cells (vehicle) and in cells pretreated with holo-RBP (RBP). Means ± S.E. ($n = 5$/group), #, $p < 0.01$ *versus* nontreated controls (*white bars*).

pocytes, 3T3-L1 cells. Cells were induced to differentiate into adipocytes using standard protocols (49, 50). 3T3-L1 adipocytes with reduced expression of STRA6 were obtained using *Stra6*-shRNA (Fig. 3*I*, *inset*). Similarly to primary adipocytes, reducing the expression of STRA6 in cultured 3T3-L1 adipocytes abolished the ability of holo-RBP to inhibit insulin-induced glucose uptake (Fig. 3*I*, *gray bars*).

Holo-RBP was then administered to WT and *Stra6*-null mice by intraperitoneal injections (1 mg of holo-RBP was injected three times at 2-h intervals, and mice were sacrificed 1 h after the last injection). Immunoblot analyses showed that RBP in serum of treated mice displayed two bands, corresponding to endogenous and recombinant His-tagged RBP, respectively (Fig. 4*A*). The injections increased the total serum level of RBP by about 1.5–2-fold, similarly to increases observed in the blood of obese mice (9). Interestingly, they also resulted in a higher level of recombinant RBP in plasma of *Stra6*-null mice, suggesting that the protein remains in the circulation longer in the absence of STRA6. Injections of holo-RBP to WT mice induced phosphorylation of JAK2 and increased the expression of two well established STAT target genes in WAT and muscle as follows: *Socs3*, a potent inhibitor of insulin signaling (25), and *Pparg*, a nuclear receptor that promotes adipogenesis and lipid accumulation (51). In contrast, injections of holo-RBP did not alter the phosphorylation status of JAK2 or the expression of either *Socs3* or *Pparg* in *Stra6*-null mice (Fig. 4, *B–I*). In accordance with up-regulation of the cytokine signaling inhibitor SOCS3, injections of holo-RBP to WT mice markedly decreased the phosphorylation level of both IR and its downstream effector AKT in WAT (Fig. 4, *F* and *G*) and skeletal muscle (Fig. 4, *H* and *I*). Strikingly, injection of holo-RBP had no effect on the phosphorylation levels of either IR or AKT in *Stra6*-null mice (Fig. 4, *F–I*). Importantly, holo-RBP injections had no effect on the phosphorylation status of JAK2, IR, or AKT in the liver, an organ that does not express STRA6 (Fig. 5). The observations thus demonstrate that STRA6 is a critical mediator of the ability of holo-RBP to suppress insulin signaling *in vivo*.

STRA6 Contributes to High Fat Diet-induced Insulin Resistance— 6-Week-old WT and *Stra6*-null male mice were fed a high fat/high sucrose diet (HFHSD) for 14 weeks, a dietary regime that leads to obesity and insulin resistance (52). Total weight gain of *Stra6*-null mice was not significantly different from that of WT littermates. HFHSD feeding resulted in similar elevation of serum RBP levels in WT and in *Stra6*-null mice (Fig. 6*A*) and induced a decreased phosphorylation status of IR and AKT in adipose tissue (Fig. 6, *B* and *C*) and muscle (Fig. 6, *D* and *E*) of both WT and *Stra6*-null mice. Notably however, the

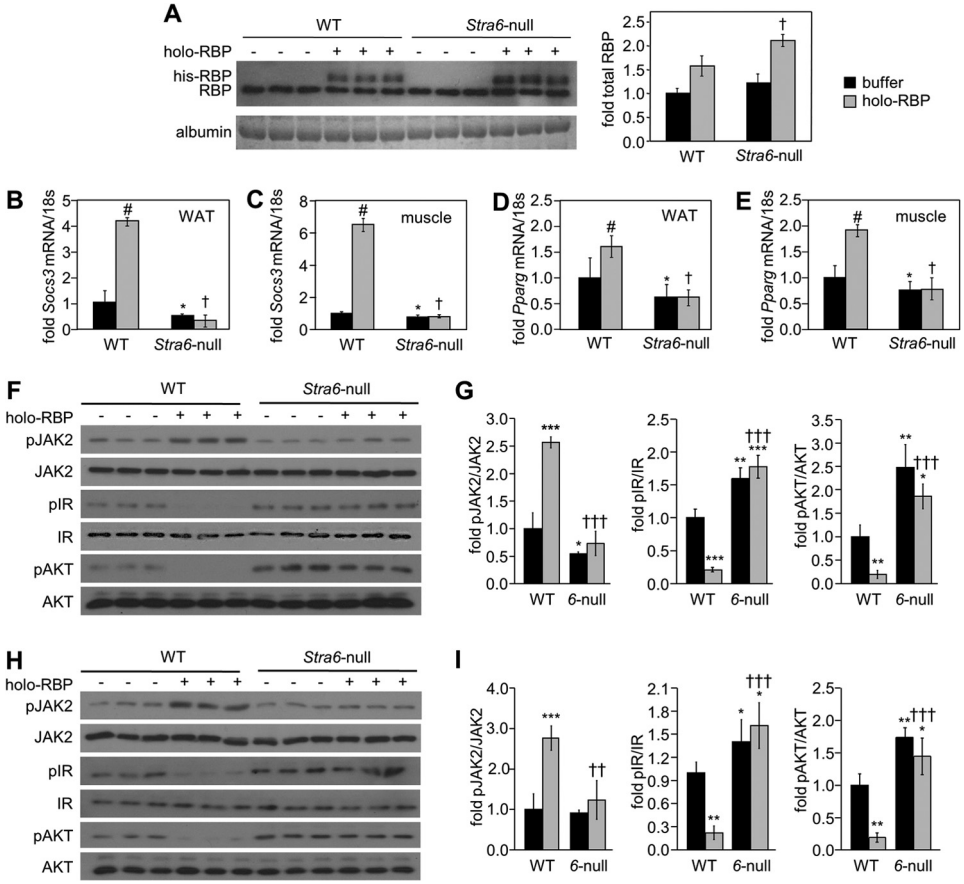

FIGURE 4. **Stra6-null mice are protected from activation of STAT and suppression of insulin signaling by holo-RBP.** *A, left panel,* immunoblots demonstrating the level of RBP in serum of three individual WT and *Stra6*-null male mice injected with buffer (−) or with recombinant histidine-tagged RBP (*holo-RBP*). Coomassie Blue staining of serum albumin provided a loading control. *Right panel,* quantitation of immunoblots showing total serum RBP levels in denoted groups. †, $p < 0.05$ holo-RBP-treated *Stra6*-null *versus* WT mice. *B–E,* levels of mRNAs for *Socs3* (*B* and *C*) and *Pparg* (*D* and *E*) in WAT (*B* and *D*) and skeletal muscle (*C* and *E*) of WT and *Stra6*-null mice treated with buffer (*black bars*) or with holo-RBP (*gray bars*). Data are means ± S.E. ($n = 3$/group). #, $p < 0.05$ holo-RBP-treated *versus* buffer-treated WT mice; *, $p < 0.05$ buffer-treated *Stra6*-null *versus* WT mice; †, $p < 0.05$ holo-RBP-treated *Stra6*-null *versus* WT mice. *F* and *H,* immunoblots of pJAK2, JAK2, pIR, IR, pAKT, and AKT in WAT (*F*) and skeletal muscle (*H*) of WT and *Stra6*-null mice (*6-null*) treated with buffer or with holo-RBP. *G* and *I,* quantitation of immunoblots in *F* and *H*, respectively. Means ± S.D. *, $p < 0.05$; **, $p < 0.01$; ***, $p < 0.001$ *versus* buffer-treated WT mice. ††, $p < 0.01$; †††, $p < 0.001$ *versus* holo-RBP-treated WT mice.

decrease in phosphorylation of IR and AKT was less pronounced in WAT and muscle of *Stra6*-null than in WT mice. In fact, the phosphorylation levels of adipose and muscle IR and AKT in obese *Stra6*-null mutant mice resembled those observed in lean WT animals (compare Fig. 6, *C* with *E*). HFHSD feeding also reduced the phosphorylation status of IR and AKT in liver, which does not express STRA6, but unlike adipose tissue and muscle, no differences were observed between the effect of HFHSD on phosphorylation of these proteins in WT and *Stra6*-null mice (Fig. 6, *F* and *G*). The data thus show that STRA6 is not the sole factor but is an important contributor to impairment of insulin signaling in obese mice. In agreement with this conclusion, glucose tolerance tests showed that obese *Stra6*-null were significantly more glucose-tolerant than their WT counterparts (Fig. 6*H*). Accordingly, hyperinsulinemic-euglycemic clamp experiments performed in conscious, unrestrained mice revealed that the GIR necessary to maintain euglycemia was significantly higher in obese *Stra6*-null mutants than in obese WT mice (Fig. 6*I*). The observations thus establish that ablation of STRA6 protects animals from HFHSD-induced insulin resistance.

DISCUSSION

STRA6, originally identified as an RA-inducible membrane protein (16), was subsequently characterized in cultured cells as a plasma membrane receptor that mediates cellular uptake of ROH from extracellular holo-RBP (15). It was recently reported that STRA6 also functions in cultured cells as a cell-surface signaling receptor that is phosphorylated upon binding of holo-RBP and, in turn, activates a JAK2/STAT5 cascade to up-regulate the expression of STAT target genes (21–24). However, whether STRA6 mediates ROH uptake and whether it is critical for maintaining proper vitamin A homeostasis *in vivo* is unknown. Similarly, whether STRA6-mediated signaling is operational and is involved in holo-RBP-induced insulin resistance *in vivo* remains to be clarified. To address these questions, we generated a *Stra6*-null mutant mouse line.

In contrast with the severe malformations correlated with *Stra6* mutations in humans suffering from Matthew-Woods syndrome (17–19), *Stra6*-null mice are morphologically normal and fertile. These observations are in agreement with the phenotype of a STRA6-null mouse line generated by Lexicon

Genetics (B6;129S5-*Stra6Gt*(*OST353837*)*Lex*355/Mmucd), which were found to exhibit decreased body weight but no other notable impairment (see Mutant Mouse Regional Resource Centers, University of California at Davis). It could be argued that the lack of overt malformations in *Stra6-null* mice may stem from the existence of a protein that functionally compensates for the lack of STRA6. Interestingly, a *Stra6* paralog displaying 40% similarity at the protein level has been identified in the mouse genome (RBP receptor 2, RBPR2 also termed 1300002K09Rik) (38). This gene is conserved among mammals except in great apes and humans in which it is split in two parts with an associated break in synteny. It could thus be argued that RBPR2 may compensate for loss of STRA6 in the mouse but not in humans. However, the following considerations indicate that RBPR2 is unlikely to compensate for *Stra6* even in the mouse: (i) the expression patterns of STRA6 and RBPR2 in the mouse do not overlap (Fig. 7, *A–F*); (ii) *Rbpr2* is neither ectopically expressed in *Stra6*-expressing tissues nor increased in other tissues of *Stra6*-null mutants (Fig. 7, *F–I*); and (iii) although RBPR2 appears to function as an ROH transporter (38), it does not possess the phosphotyrosine residue or the signaling features of STRA6. Indeed, RBP does not activate a JAK/STAT cascade in liver, which expresses RBPR2 (Fig. 5) (21). Notably, when fed regular chow, the phenotype of mice lacking STRA6 described here and in Ref. 26 resembles that of mice lacking RBP (6, 9). These observations support the notion that the two proteins function in concert and suggest that STRA6 does not have biological activities that are independent of its cooperation with RBP. The discrepancy between the mild symptoms displayed by humans carrying RBP mutations (20) and the severe symptoms displayed by humans suffering from Matthew-Woods syndrome (17–19) thus raise the possibility that Matthew-Woods syndrome is not caused primarily by loss of STRA6 function but involves additional genetic alterations. It is interesting to note in regard to this that no mutations in *STRA6*

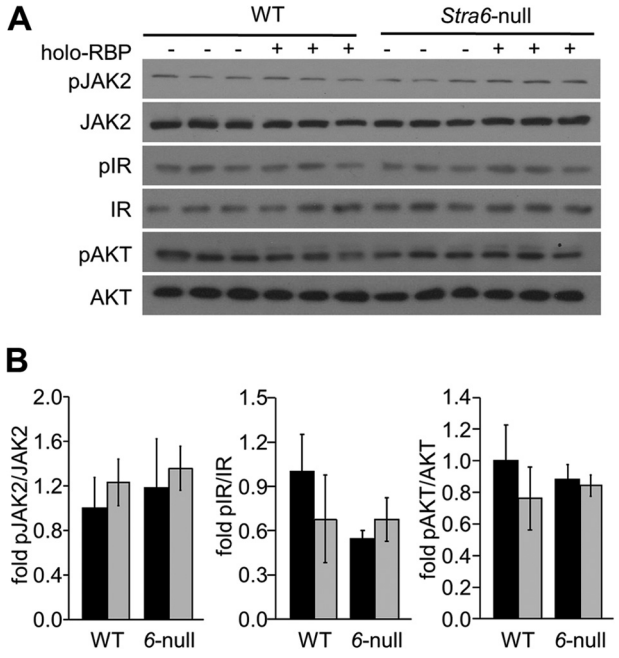

FIGURE 5. **Holo-RBP does not alter insulin signaling in the liver.** *A,* immunoblots of pJAK2, JAK2, pIR, IR, pAKT, and AKT in liver of WT and *Stra6*-null mice (*6-null*) treated with buffer or with holo-RBP. *B,* quantitation of immunoblots in *A*. Means ± S.D.

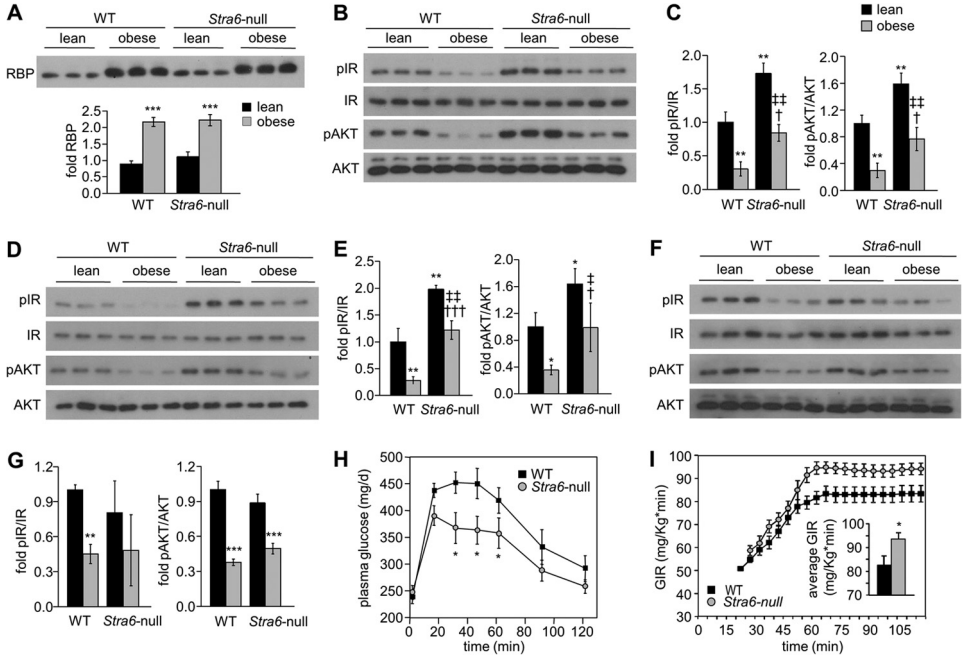

FIGURE 6. **Stra6 contributes to diet-induced insulin resistance.** *A,* immunoblots of RBP in serum of three individual WT and *Stra6*-null male mice fed normal chow (*lean*) or fed an HFHS diet for 14 weeks (*obese*). Mean ± S.D., ***, $p < 0.001$ *versus* lean WT mice. *B, D,* and *F,* immunoblots of pIR, IR, pAKT, and AKT in WAT (*B*), skeletal muscle (*D*), and liver (*F*) of three individual WT and *Stra6*-null male mice fed regular chow (*lean*) or an HFHS diet (*obese)* for 14 weeks. *C, E,* and *G,* quantitation of immunoblots in *B, D,* and *F,* respectively. Mean ± S.D., *, $p < 0.05$; **, $p < 0.01$, *versus* lean WT mice; †, $p < 0.05$; †††, $p < 0.001$ *versus* obese WT mice; ‡, $p < 0.05$; ‡‡, $p < 0.01$ *versus* obese *Stra6*-null mice. *H,* glucose tolerance test in WT ($n = 11$) and *Stra6*-null ($n = 12$) males following 10 weeks feeding an HFHS diet. Means ± S.E. *, $p < 0.05$ WT *versus Stra6*-null mice. The calculated area under the curve (*AUC*) was 45,505 mg/dl·min and 39,091 mg/dl·min for WT and *Stra6*-null mice, respectively. *I,* GIR in WT and *Stra6*-null mice fed an HFHSD for 10 weeks and subjected to hyperinsulinemic-euglycemic clamp. *Inset,* average GIR between $t = 60$ min and $t = 120$ min. Means ± S.E. ($n = 9$ or 10/group). *, $p < 0.05$ WT *versus Stra6*-null mice.

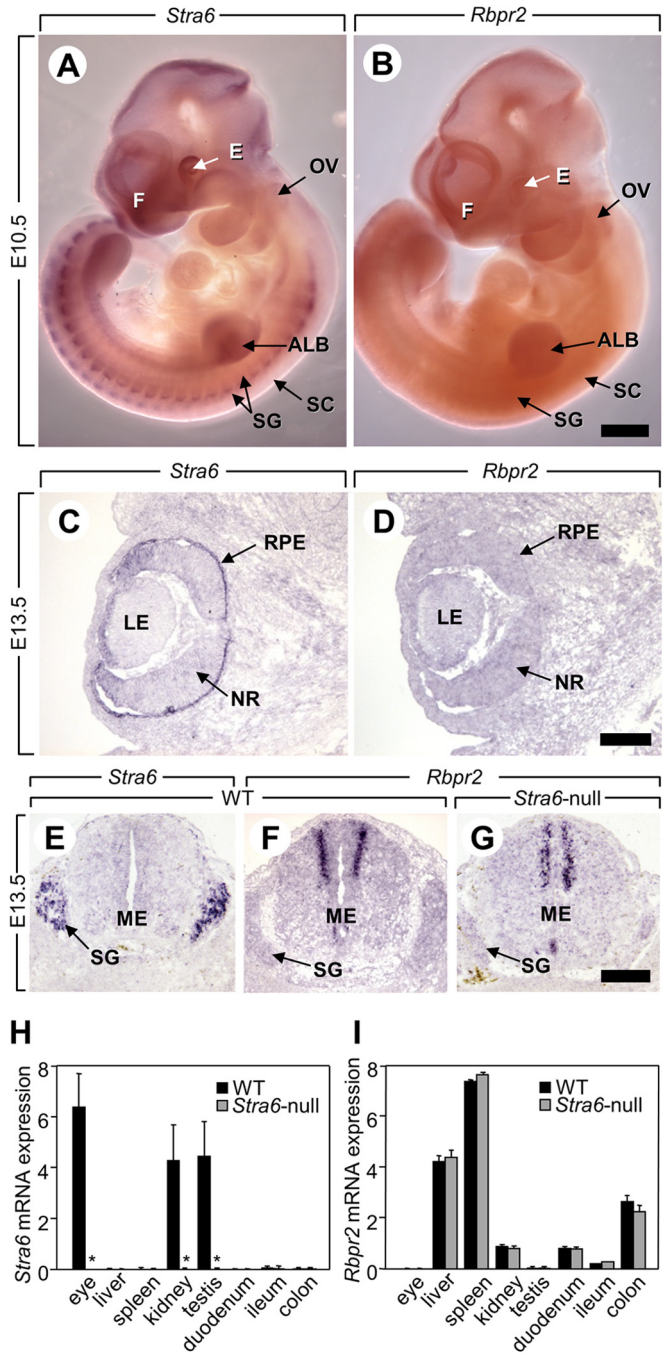

FIGURE 7. **Expressions of *Stra6* and *Rbpr2* do not overlap, and *Rbpr2* expression is not altered in *Stra6*-null mutants to compensate for the loss of STRA6.** *A* and *B*, whole mounts of embryos at embryonic day 10.5 (*E10.5*). *Stra6* is expressed in many tissues (*e.g. purple* signal in the eye, the forebrain), whereas *Rbpr2* is not detectable at this stage. *Scale bar* in *B*, 1 mm. *C–F*, histological sections of a WT fetus at E13.5. Strong expression of *Stra6* (*purple* signal) is detected in the retinal pigment epithelium (*C*) and in the spinal ganglia (*G*), which do not express *Rbpr2* (*D*). In contrast, strong expression of *Rbpr2* is detected in the dorsal portion of the medulla (*F*), which does not express *Stra6* (*E*). *G*, histological sections of a *Stra6*-null fetus at E13.5. *Rbpr2* is not ectopically expressed in the spinal ganglia when *Stra6* is ablated. *Scale bars* in *D* and *G*: 300 μm. Legend: *ALB*, anterior limb bud; *E*, eye; *F*, forebrain; *LE*, lens; *ME*, medulla; *NR*, neural retina; *OV*, otic vesicle; *RPE*, retinal pigment epithelium; *SC*, spinal cord; *SG*, spinal ganglion. *H* and *I*, levels of mRNAs coding for *Stra6* (*H*) and *Rbpr2* (*I*) in STRA6-expressing tissues (*e.g.* eye, kidney, and testis) and RBRP2-expressing tissues (*e.g.* liver, spleen, kidney, duodenum, ileum, and colon) of 12 week-old WT (*black bars*) and *Stra6*-null (*gray bars*) mice. Data are means ± S.E. ($n = 4$/group), *, $p < 0.05$ *Stra6*-null *versus* WT mice. As expected, no *Stra6* mRNA is detected in *Stra6*-null mice. Importantly, *Rbpr2* expression is not increased in mutant tissues normally expressing *Stra6* (*e.g.* eye, kidney, and testis).

gene were found in a patient suffering PAGOD syndrome, a multiple congenital anomalies syndrome, including defects in vitamin A homeostasis, which presents significant phenotypic overlap with Matthew-Woods syndrome (53).

Our studies provide several lines of evidence that establish that, with the exception of the eye, STRA6 is not critical for maintaining ROH availability in tissues that express it. (i) The retinoid content of tissues is indistinguishable in *Stra6*-null and WT mice fed a regular chow diet. (ii) *Stra6*-null fetuses recovered from dams fed a VADD do not exhibit any hallmarks of fetal VAD syndrome. Accordingly, RA signaling is not affected by the absence of STRA6, except in the eye, as assessed by the expression patterns of a sensitive RA-inducible reporter in WT and *Stra6*-null mice. In addition to its proposed function in enabling ROH entry into STRA6-expressing cells, it was proposed that the receptor can mediate efflux of ROH, thereby reducing the teratogenic potency of ROH during embryonic development (43). Our data show however that WT and *Stra6*-null fetuses display identical manifestations of ROH-induced teratogenesis and that mice lacking both STRA6 and the ROH-esterifying enzyme lecithin-retinol acyltransferase are not more sensitive to ROH excess than mice lacking lecithin-retinol acyltransferase only. Altogether, the data indicate that STRA6 is not critical for maintaining adequate ROH content in most tissues. The exception is the eye where, due to a high retinoid turnover rate and the very high expression level of the receptor in RPE, ablation of STRA6 leads to severe depletion of retinoid stores. Notably, even in this sensitive organ, morphological changes and reduction in visual function are mild in *Stra6*-null mice, indicating that STRA6 is not the only pathway by which ROH enters the RPE (26).

The rate of uptake of ROH from circulating holo-RBP and the retinoid content of STRA6-expressing tissues in mice fed a vitamin A-deficient diet, rendering holo-RBP the sole source of ROH, were modestly but significantly reduced in *Stra6*-null mice. The small magnitude of the effects shows that ROH can readily move from circulating holo-RBP into cells in the absence of STRA6. Indeed, in contrast to the critical need for RBP for development in mice fed VADD (8), *Stra6*-null fetuses from *Stra6*-null dams fed a VADD do not exhibit any hallmarks of fetal VAD syndrome. These observations strongly support the conclusion that the major fraction of cellular uptake of ROH from circulating holo-RBP occurs in a transporter-independent fashion, likely by diffusion across the plasma membrane, at rates that are sufficient for physiological needs. Nevertheless, the data show that STRA6 indeed mediates ROH uptake *in vivo*. Considering that ROH transport and signaling by STRA6 are critically inter-dependent (24), an attractive possibility is that, rather than simply supplying cells with vitamin A, ROH transport by STRA6 in tissues other than the eye serves mainly to allow the activation of STRA6 signaling.

In support of the notion that STRA6 mediates the ability of holo-RBP to induce insulin resistance and that it does so by activating a JAK2/STAT cascade (21), administration of holo-RBP induced the phosphorylation of JAK2, increased the expression of STAT target genes, and reduced the activation of IR in WAT and muscle of WT mice but had no effect on these parameters in *Stra6*-null animals. In accordance, holo-RBP

inhibited insulin-stimulated glucose uptake by primary adipocytes isolated from WT mice, but it did not hamper insulin-stimulated glucose uptake by adipocytes isolated from *Stra6*-null animals. Moreover, despite similar elevation in serum RBP levels, glucose tolerance tests and hyperinsulinemic-euglycemic clamp experiments showed that obese *Stra6*-null mice are significantly more insulin-responsive than their WT counterparts. The data thus demonstrate that STRA6 plays a key role in the impairment of insulin signaling brought about upon high fat feeding. Nevertheless, it is worth noting that although the effect was significantly smaller than that observed in WT mice, HFHSD consumption did result in a decrease in the phosphorylation status of IR and AKT in *Stra6*-null animals, and such an effect was also observed in liver that does not express STRA6. Hence, holo-RBP/STRA6 signaling is not the sole mechanism that underlies the link between obesity and insulin resistance. One candidate for exerting such an effect is leptin, another adipokine whose expression is elevated in obese animals and that, like RBP, activates JAK/STAT signaling and impairs insulin signaling in tissues that express the leptin receptor (54).

Taken together, the data demonstrate that, upon binding of holo-RBP, STRA6 mediates ROH uptake, activates JAK2/STAT signaling, and suppresses insulin responses *in vivo*. The observations further show that STRA6-mediated ROH uptake is not necessary for supplying target tissues, except the RPE, with physiological amounts of ROH. Hence, with the exception of the eye, the function of STRA6 *in vivo* appears to couple sensing of circulating holo-RBP levels to cell signaling that, in turn, allows the regulation of key processes such as insulin response.

Acknowledgments—We are grateful to L. El Fertak and R. Combe who performed and analyzed the hyperinsulinemic-euglycemic clamp experiments in the Phenotyping Department of the Mouse Clinical Institute of Illkirch. The Mouse Metabolic Phenotyping Center of Case Western Reserve University is supported by National Institutes of Health Grant DK59630. The Stra6-null mouse line was established at the Mouse Clinic Institute in the Genetic Engineering and Model Validation Department of Inserm and supported by Fondation pour la Recherche Médicale Grant DEQ20071210544 (to N. B. G. and M. M.).

REFERENCES

1. Wilson, J. G., Roth, C. B., and Warkany, J. (1953) An analysis of the syndrome of malformations induced by maternal vitamin A deficiency. Effects of restoration of vitamin A at various times during gestation. *Am. J. Anat.* **92,** 189–217
2. Wald, G. (1968) The molecular basis of visual excitation. *Nature* **219,** 800–807
3. Mark, M., Ghyselinck, N. B., and Chambon, P. (2006) Function of retinoid nuclear receptors: lessons from genetic and pharmacological dissections of the retinoic acid signaling pathway during mouse embryogenesis. *Annu. Rev. Pharmacol. Toxicol.* **46,** 451–480
4. Schug, T. T., Berry, D. C., Shaw, N. S., Travis, S. N., and Noy, N. (2007) Opposing effects of retinoic acid on cell growth result from alternate activation of two different nuclear receptors. *Cell* **129,** 723–733
5. Quadro, L., Hamberger, L., Colantuoni, V., Gottesman, M. E., and Blaner, W. S. (2003) Understanding the physiological role of retinol-binding protein in vitamin A metabolism using transgenic and knockout mouse models. *Mol. Aspects Med.* **24,** 421–430
6. Quadro, L., Blaner, W. S., Salchow, D. J., Vogel, S., Piantedosi, R., Gouras, P., Freeman, S., Cosma, M. P., Colantuoni, V., and Gottesman, M. E. (1999) Impaired retinal function and vitamin A availability in mice lacking retinol-binding protein. *EMBO J.* **18,** 4633–4644
7. Ghyselinck, N. B., Vernet, N., Dennefeld, C., Giese, N., Nau, H., Chambon, P., Viville, S., and Mark, M. (2006) Retinoids and spermatogenesis: lessons from mutant mice lacking the plasma retinol-binding protein. *Dev. Dyn.* **235,** 1608–1622
8. Quadro, L., Hamberger, L., Gottesman, M. E., Wang, F., Colantuoni, V., Blaner, W. S., and Mendelsohn, C. L. (2005) Pathways of vitamin A delivery to the embryo: insights from a new tunable model of embryonic vitamin A deficiency. *Endocrinology* **146,** 4479–4490
9. Yang, Q., Graham, T. E., Mody, N., Preitner, F., Peroni, O. D., Zabolotny, J. M., Kotani, K., Quadro, L., and Kahn, B. B. (2005) Serum retinol-binding protein 4 contributes to insulin resistance in obesity and type 2 diabetes. *Nature* **436,** 356–362
10. Noy, N. (2000) Retinoid-binding proteins: mediators of retinoid action. *Biochem. J.* **348,** 481–495
11. Fex, G., and Johannesson, G. (1988) Retinol transfer across and between phospholipid bilayer membranes. *Biochim. Biophys. Acta* **944,** 249–255
12. Noy, N., and Xu, Z. J. (1990) Kinetic parameters of the interactions of retinol with lipid bilayers. *Biochemistry* **29,** 3883–3888
13. Heller, J. (1975) Interactions of plasma retinol-binding protein with its receptor. Specific binding of bovine and human retinol-binding protein to pigment epithelium cells from bovine eyes. *J. Biol. Chem.* **250,** 3613–3619
14. Shingleton, J. L., Skinner, M. K., and Ong, D. E. (1989) Characteristics of retinol accumulation from serum retinol-binding protein by cultured Sertoli cells. *Biochemistry* **28,** 9641–9647
15. Kawaguchi, R., Yu, J., Honda, J., Hu, J., Whitelegge, J., Ping, P., Wiita, P., Bok, D., and Sun, H. (2007) A membrane receptor for retinol-binding protein mediates cellular uptake of vitamin A. *Science* **315,** 820–825
16. Bouillet, P., Sapin, V., Chazaud, C., Messaddeq, N., Décimo, D., Dollé, P., and Chambon, P. (1997) Developmental expression pattern of Stra6, a retinoic acid-responsive gene encoding a new type of membrane protein. *Mech. Dev.* **63,** 173–186
17. Pasutto, F., Sticht, H., Hammersen, G., Gillessen-Kaesbach, G., Fitzpatrick, D. R., Nürnberg, G., Brasch, F., Schirmer-Zimmermann, H., Tolmie, J. L., Chitayat, D., Houge, G., Fernández-Martínez, L., Keating, S., Mortier, G., Hennekam, R. C., von der Wense, A., Slavotinek, A., Meinecke, P., Bitoun, P., Becker, C., Nürnberg, P., Reis, A., and Rauch, A. (2007) Mutations in STRA6 cause a broad spectrum of malformations including anophthalmia, congenital heart defects, diaphragmatic hernia, alveolar capillary dysplasia, lung hypoplasia, and mental retardation. *Am. J. Hum. Genet.* **80,** 550–560
18. Golzio, C., Martinovic-Bouriel, J., Thomas, S., Mougou-Zrelli, S., Grattagliano-Bessieres, B., Bonniere, M., Delahaye, S., Munnich, A., Encha-Razavi, F., Lyonnet, S., Vekemans, M., Attie-Bitach, T., and Etchevers, H. C. (2007) Matthew-Wood syndrome is caused by truncating mutations in the retinol-binding protein receptor gene STRA6. *Am. J. Hum. Genet.* **80,** 1179–1187
19. Chassaing, N., Golzio, C., Odent, S., Lequeux, L., Vigouroux, A., Martinovic-Bouriel, J., Tiziano, F. D., Masini, L., Piro, F., Maragliano, G., Delezoide, A. L., Attié-Bitach, T., Manouvrier-Hanu, S., Etchevers, H. C., and Calvas, P. (2009) Phenotypic spectrum of STRA6 mutations: from Matthew-Wood syndrome to non-lethal anophthalmia. *Hum. Mutat.* **30,** E673–E681
20. Biesalski, H. K., Frank, J., Beck, S. C., Heinrich, F., Illek, B., Reifen, R., Gollnick, H., Seeliger, M. W., Wissinger, B., and Zrenner, E. (1999) Biochemical but not clinical vitamin A deficiency results from mutations in the gene for retinol-binding protein. *Am. J. Clin. Nutr.* **69,** 931–936
21. Berry, D. C., Jin, H., Majumdar, A., and Noy, N. (2011) Signaling by vitamin A and retinol-binding protein regulates gene expression to inhibit insulin responses. *Proc. Natl. Acad. Sci. U.S.A.* **108,** 4340–4345
22. Berry, D. C., and Noy, N. (2012) Signaling by vitamin A and retinol-binding protein in regulation of insulin responses and lipid homeostasis. *Biochim. Biophys. Acta* **1821,** 168–176
23. Berry, D. C., Croniger, C. M., Ghyselinck, N. B., and Noy, N. (2012) Transthyretin blocks retinol uptake and cell signalling by the holo-retinol-

binding protein receptor STRA6. *Mol. Cell. Biol.* **32,** 3851–3859
24. Berry, D. C., O'Byrne, S. M., Vreeland, A. C., Blaner, W. S., and Noy, N. (2012) Cross talk between signaling and vitamin A transport by the retinol-binding protein receptor STRA6. *Mol. Cell. Biol.* **32,** 3164–3175
25. Starr, R., Willson, T. A., Viney, E. M., Murray, L. J., Rayner, J. R., Jenkins, B. J., Gonda, T. J., Alexander, W. S., Metcalf, D., Nicola, N. A., and Hilton, D. J. (1997) A family of cytokine-inducible inhibitors of signalling. *Nature* **387,** 917–921
26. Ruiz, A., Mark, M., Jacobs, H., Klopfenstein, M., Hu, J., Lloyd, M., Habib, S., Tosha, C., Radu, R. A., Ghyselinck, N. B., Nusinowitz, S., and Bok, D. (2012) Retinoid content, visual responses, and ocular morphology are compromised in the retinas of mice lacking the retinol-binding protein receptor, STRA6. *Invest. Ophthalmol. Vis. Sci.* **53,** 3027–3039
27. Rodríguez, C. I., Buchholz, F., Galloway, J., Sequerra, R., Kasper, J., Ayala, R., Stewart, A. F., and Dymecki, S. M. (2000) High-efficiency deleter mice show that FLPe is an alternative to Cre-loxP. *Nat. Genet.* **25,** 139–140
28. Dupé, V., Davenne, M., Brocard, J., Dollé, P., Mark, M., Dierich, A., Chambon, P., and Rijli, F. M. (1997) *In vivo* functional analysis of the Hoxa-1 3′-retinoic acid response element (3′RARE). *Development* **124,** 399–410
29. Antal, C., Teletin, M., Wendling, O., Dgheem, M., Auwerx, J., and Mark, M. (2007) Tissue collection for systematic phenotyping in the mouse. *Curr. Protoc. Mol. Biol.* Chapter 29, Unit 29A.4
30. Vernet, N., Dennefeld, C., Guillou, F., Chambon, P., Ghyselinck, N. B., and Mark, M. (2006) Prepubertal testis development relies on retinoic acid but not rexinoid receptors in Sertoli cells. *EMBO J.* **25,** 5816–5825
31. Sanes, J. R., Rubenstein, J. L., and Nicolas, J. F. (1986) Use of a recombinant retrovirus to study post-implantation cell lineage in mouse embryos. *EMBO J.* **5,** 3133–3142
32. Wei, S., Episkopou, V., Piantedosi, R., Maeda, S., Shimada, K., Gottesman, M. E., and Blaner, W. S. (1995) Studies on the metabolism of retinol and retinol-binding protein in transthyretin-deficient mice produced by homologous recombination. *J. Biol. Chem.* **270,** 866–870
33. Blaner, W. S., Das, S. R., Gouras, P., and Flood, M. T. (1987) Hydrolysis of 11-cis- and all-*trans*-retinyl palmitate by homogenates of human retinal epithelial cells. *J. Biol. Chem.* **262,** 53–58
34. Amengual, J., Golczak, M., Palczewski, K., and von Lintig, J. (2012) Lecithin:retinol acyltransferase is critical for cellular uptake of vitamin A from serum retinol-binding protein. *J. Biol. Chem.* **287,** 24216–24227
35. Ruan, H., Zarnowski, M. J., Cushman, S. W., and Lodish, H. F. (2003) Standard isolation of primary adipose cells from mouse epididymal fat pads induces inflammatory mediators and down-regulates adipocyte genes. *J. Biol. Chem.* **278,** 47585–47593
36. Ayala, J. E., Bracy, D. P., McGuinness, O. P., and Wasserman, D. H. (2006) Considerations in the design of hyperinsulinemic-euglycemic clamps in the conscious mouse. *Diabetes* **55,** 390–397
37. Kawaguchi, R., Yu, J., Wiita, P., Ter-Stepanian, M., and Sun, H. (2008) Mapping the membrane topology and extracellular ligand binding domains of the retinol-binding protein receptor. *Biochemistry* **47,** 5387–5395
38. Alapatt, P., Guo, F., Komanetsky, S. M., Wang, S., Cai, J., Sargsyan, A., Rodríguez Díaz, E., Bacon, B. T., Aryal, P., and Graham, T. E. (2013) Liver retinol transporter and receptor for serum retinol-binding protein (RBP4). *J. Biol. Chem.* **288,** 1250–1265
39. Mark, M., Teletin, M., Antal, C., Wendling, O., Auwerx, J., Heikkinen, S., Khetchoumian, K., Argmann, C. A., and Dgheem, M. (2007) Histopathology in mouse metabolic investigations. *Curr. Protoc. Mol. Biol.* Chapter 29, Unit 29B.4
40. Rossant, J., Zirngibl, R., Cado, D., Shago, M., and Giguère, V. (1991) Expression of a retinoic acid response element-hsplacZ transgene defines specific domains of transcriptional activity during mouse embryogenesis. *Genes Dev.* **5,** 1333–1344
41. Niederreither, K., and Dollé, P. (2008) Retinoic acid in development: towardan integrated view. *Nat. Rev. Genet.* **9,** 541–553
42. Duester, G. (2008) Retinoic acid synthesis and signaling during early organogenesis. *Cell* **134,** 921–931
43. Isken, A., Golczak, M., Oberhauser, V., Hunzelmann, S., Driever, W., Imanishi, Y., Palczewski, K., and von Lintig, J. (2008) RBP4 disrupts vitamin A uptake homeostasis in a STRA6-deficient animal model for Matthew-Wood syndrome. *Cell Metab.* **7,** 258–268
44. Geelen, J. A. (1979) Hypervitaminosis A induced teratogenesis. *CRC Crit. Rev. Toxicol.* **6,** 351–375
45. Kim, Y. K., Wassef, L., Hamberger, L., Piantedosi, R., Palczewski, K., Blaner, W. S., and Quadro, L. (2008) Retinyl ester formation by lecithin: retinol acyltransferase is a key regulator of retinoid homeostasis in mouse embryogenesis. *J. Biol. Chem.* **283,** 5611–5621
46. Ruiz, A., Ghyselinck, N. B., Mata, N., Nusinowitz, S., Lloyd, M., Dennefeld, C., Chambon, P., and Bok, D. (2007) Somatic ablation of the *Lrat* gene in the mouse retinal pigment epithelium drastically reduces its retinoid storage. *Invest. Ophthalmol. Vis. Sci.* **48,** 5377–5387
47. Soprano, D. R., Pickett, C. B., Smith, J. E., and Goodman, D. S. (1981) Biosynthesis of plasma retinol-binding protein in liver as a larger molecular weight precursor. *J. Biol. Chem.* **256,** 8256–8258
48. Xie, Y., Lashuel, H. A., Miroy, G. J., Dikler, S., and Kelly, J. W. (1998) Recombinant human retinol-binding protein refolding, native disulfide formation, and characterization. *Protein Expr. Purif.* **14,** 31–37
49. Green, H., and Kehinde, O. (1975) An established preadipose cell line and its differentiation in culture. II. Factors affecting the adipose conversion. *Cell* **5,** 19–27
50. Green, H., and Meuth, M. (1974) An established pre-adipose cell line and its differentiation in culture. *Cell* **3,** 127–133
51. Lehrke, M., and Lazar, M. A. (2005) The many faces of PPARγ. *Cell* **123,** 993–999
52. Wang, C. Y., and Liao, J. K. (2012) A mouse model of diet-induced obesity and insulin resistance. *Methods Mol. Biol.* **821,** 421–433
53. Gavrilova, R., Babovic, N., Lteif, A., Eidem, B., Kirmani, S., Olson, T., and Babovic-Vuksanovic, D. (2009) Vitamin A deficiency in an infant with PAGOD syndrome. *Am. J. Med. Genet. A* **149A,** 2241–2247
54. Cirillo, D., Rachiglio, A. M., la Montagna, R., Giordano, A., and Normanno, N. (2008) Leptin signaling in breast cancer: an overview. *J. Cell. Biochem.* **105,** 956–964